# Pressure and temperature dependence of dissociative and non-dissociative electron attachment to CF3: Experiments and kinetic modeling

Nicholas S. Shuman, Thomas M. Miller, Jeffrey F. Friedman, Albert A. Viggiano, Anatol I. Maergoiz et al.

Citation: J. Chem. Phys. **135**, 054306 (2011); doi: 10.1063/1.3614471
View online: http://dx.doi.org/10.1063/1.3614471
View Table of Contents: http://jcp.aip.org/resource/1/JCPSA6/v135/i5
Published by the American Institute of Physics.

# Pressure and temperature dependence of dissociative and non-dissociative electron attachment to $CF_3$: Experiments and kinetic modeling

Nicholas S. Shuman,[1] Thomas M. Miller,[1] Jeffrey F. Friedman,[1] Albert A. Viggiano,[1] Anatol I. Maergoiz,[2] and Jürgen Troe[2,3,a)]
[1]*Air Force Research Laboratory, Space Vehicles Directorate, 3550 Aberdeen Avenue SE, Bldg 570, Kirtland Air Force Base, New Mexico 87117-5776, USA*
[2]*Institut für Physikalische Chemie, Universität Göttingen, Tammannstrasse 6, D-37077 Göttingen, Germany*
[3]*Max-Planck-Institut für biophysikalische Chemie, Am Fassberg 11, D-37077 Göttingen, Germany*

(Received 13 May 2011; accepted 30 June 2011; published online 3 August 2011)

The kinetics of electron attachment to $CF_3$ as a function of temperature (300–600 K) and pressure (0.75–2.5 Torr) were studied by variable electron and neutral density attachment mass spectrometry exploiting dissociative electron attachment to $CF_3Br$ as a radical source. Attachment occurs through competing dissociative ($CF_3 + e^- \rightarrow CF_2 + F^-$) and non-dissociative channels ($CF_3 + e^- \rightarrow CF_3^-$). The rate constant of the dissociative channel increases strongly with temperature, while that of the non-dissociative channel decreases. The rate constant of the non-dissociative channel increases strongly with pressure, while that of the dissociative channel shows little dependence. The total rate constant of electron attachment increases with temperature and with pressure. The system is analyzed by kinetic modeling in terms of statistical theory in order to understand its properties and to extrapolate to conditions beyond those accessible in the experiment. © *2011 American Institute of Physics*. [doi:10.1063/1.3614471]

## I. INTRODUCTION

Industrial fabrication of semiconductor devices relies on plasma etching, a process in which semiconductor material is selectively removed by exposure to a plasma, typically produced from a mixture of fluorocarbon gases. Etching depends on the efficiency with which the semiconductor is volatized by chemical interaction with species present in the plasma. Significant effort has been made to both identify those species and detail their associated chemistry.[1] In general, insufficient data exist to predictively model these plasma etching systems, a roadblock in achieving tighter performance tolerances required to meet rising chip densities.

In a plasma environment, fluorocarbons undergo dissociative electron attachment (DEA), dissociative ionization, and possibly thermal dissociation, all producing fluorocarbon radicals. The radicals are highly reactive species and the concentrations of $CF_n$ species are known to significantly affect the plasma etching process.[2] As a result, the plasma chemistry involving fluorocarbon radicals is of interest, but, due to the technical difficulties arising from the transient nature of the radicals, few experimental rate constants have been reported in the literature. In particular, data on the kinetics of electron attachment to fluorocarbon radicals are limited to a single beam study, placing an upper limit on the cross section for dissociative attachment to $CF_2$ at $5 \times 10^{-20}$ cm$^2$.[3] No experimental studies are available to evaluate conflicting conclusions reached by theoretical studies on electron attachment to $CF_3$. *Ab initio* and density functional calculations suggest that DEA to $CF_3$ is thermodynamically possible, but give no indication to the efficiency of the process.[4] R-matrix calculations suggest that $CF_3$ will not undergo DEA due to a lack of low-lying resonances.[5] This has important consequences for plasma etching processes: along with affecting the ion chemistry in a plasma, anions do not participate in chemistry at the etching surface due to repulsion by an electronegative sheath, while radical species, which would be produced by DEA of $CF_3$ contribute significantly.

We have recently developed[6] a novel flowing afterglow technique, variable electron and neutral density attachment mass spectrometry (VENDAMS), which allows for measurement of the kinetics of thermal electron attachment to radical species. Here, we report rate constants and product branching fractions for electron attachment to $CF_3$ over a temperature range 300–600 K and a pressure range 0.75–2.5 Torr. These data can be analyzed, using kinetic modeling in terms of statistical rate theory, to determine the underlying fundamentals of the electron attachment. Although several of the required molecular parameters are still unknown, it allows for extrapolation of the results to temperature and pressure regimes beyond those accessible by the experiment. In particular, the plasma conditions most relevant to etching (non-thermal plasmas with molecular species at 300–600 K, electron temperatures reaching up to $10^4$ K, and at low pressures, below 10 Torr) may be confidently extrapolated to.

Electron attachment to $CF_3$ is best described by a series of fundamental reaction steps analogous to those thoroughly detailed for the closed-shell species $SF_6$ and $POCl_3$ (Refs. 7–10 and 11–13, respectively). Initial capture of an

a)Author to whom correspondence should be addressed. Electronic mail: shoff@gwdg.de.

 

electron leads to an excited anionic state,

$$CF_3 + e^- \rightarrow CF_3^{-*}. \quad (1)$$

This excited state will proceed through one of the several competing processes,

$$CF_3^{-*} \rightarrow CF_3 + e^-, \quad (2)$$

$$CF_3^{-*} + M \rightarrow CF_3^- + M, \quad (3)$$

$$CF_3^{-*} \rightarrow CF_2 + F^-. \quad (4)$$

Autodetachment (2) can be identified experimentally as an increase of the total electron attachment rate constant $k_{tot}$ with increasing pressure. Non-dissociative (3) stabilization through collisions with a neutral species M depends on both the quenching efficiency of those collisions and the system pressure. The exothermicity of the overall process (1) + (3) is given by the electron affinity of $CF_3$, EA = 1.820 ± 0.050 eV.[14] Dissociation (4) through unimolecular decay is dependent on the internal energy distribution of $CF_3^{-*}$, i.e., the system behaves like a chemically activated unimolecular reaction. The overall process (1) + (4) is endothermic by 0.22 ± 0.02 eV.[15]

## II. EXPERIMENTAL METHOD AND RESULTS

Both the flowing afterglow apparatus and the VENDAMS methodology have been described in detail in Ref. 6. The apparatus consists of a 1 m long, stainless steel-lined, 7 cm diameter glass tube through which He gas is continuously flowed at a velocity of about 100 m $s^{-1}$, maintaining a pressure on the order of 1 Torr. At the upstream end of the flow, a microwave discharge excites He producing $He^+$, $He_2^+$, and $He^*$. A smaller flow of Ar (typically 5% of the He flow) is introduced several cm downstream. Collisions with Ar from $He_2^+$ and $He^*$ lead to $Ar^+$ with high efficiency. Under typical conditions, the positive charge of the resulting electron/ion plasma consists of ~95% $Ar^+$ with the remainder $He^+$, $H_2O^+$, and trace $Ar_2^+$. A 2.5 cm diameter glass ring inlet halfway down the flow tube allows for the introduction of neutral gas species into the established $Ar^+/e^-$ plasma. The charge density of the plasma can be varied between $10^7$ $cm^{-3}$ and $5 \times 10^{10}$ $cm^{-3}$ at the neutral inlet by moving the microwave cavity further from or closer to the fixed inlet as well as varying the flow rate of He through the discharge (while adjusting a complimentary flow of He downstream of the discharge in order to maintain a constant number density). The electron density is measured using a movable Langmuir probe, a 7 mm length of 25 $\mu$m diameter tungsten wire protruding from a glass sheath. The Langmuir probe is centered on the axis of the flow tube and is movable from 20 cm before to 40 cm after the neutral inlet. A 0.33 mm diameter, on axis aperture at the end of the flow tube, 46 cm past the neutral inlet, admits the gas to a quadrupole mass spectrometer used to measure the relative concentrations of ions in the flow. Mass discrimination in the mass spectrometer is accounted for through procedures described in Ref. 6. Of the species relevant to the current study, $Br^-$, $F^-$, and $CF_3^-$, mass discrimination factors of the halogen ions are measured directly, while the mass discrimination factor of the $CF_3^-$ is inferred from a calibration curve of other polyatomic anions. The velocity of the plasma between the neutral inlet and the sampling aperture is measured by pulsing the microwave discharge and noting the arrival time of the pulse as a function of distance along the flow tube using the Langmuir probe. The ambipolar diffusion rate constant in the $Ar^+/e^-$ plasma is determined by measuring the electron density as a function of distance along the flow tube with no reactant gas introduced. A typical electron diffusion rate constant at 300 K and 1 Torr was 250 $s^{-1}$, increasing roughly linearly with temperature. When electrons are present, the positive ion diffusion rate is assumed to be the same in order to maintain plasma neutrality, while anions are assumed to not diffuse significantly. When the electron density is zero, both positive and negative ions are assumed to diffuse with one half the measured electron diffusion rate constant.[16] The flow tube is wrapped with heating tape and insulated such that the temperature can be varied between room temperature and 600 K. Three resistive temperature devices along the inside wall of the flow tube have been calibrated using a movable thermocouple such that the flow tube may be heated to a constant temperature along the center axis between the neutral inlet and the sampling aperture. Prior to reaching the inlet, neutral gases pass through 50 cm of glass tubing located inside the flow tube in order to thermalize the gases at the flow tube temperature.

Measurement of plasma kinetics involving radical species in VENDAMS relies on introducing an appropriate neutral precursor to the plasma. The neutral precursor, in this case $CF_3Br$, undergoes rapid dissociative electron attachment thereby acting as a radical source. Thermal electron attachment to $CF_3Br$ between 300 and 600 K has been extensively studied and proceeds exclusively by

$$CF_3Br + e^- \rightarrow CF_3 + Br^-. \quad (5)$$

The rate constant of reaction (5) increases from $1.4 \times 10^{-8}$ $cm^3$ $s^{-1}$ at 300 K to $6.5 \times 10^{-8}$ $cm^3$ $s^{-1}$ at 600 K (see Ref. 17 and references cited therein). $CF_3Br$ is introduced in low concentrations, typically $3 \times 10^9$ $cm^{-3}$, by flowing a 0.1% mixture of $CF_3Br$ in He through a mass flowmeter at 1–2 standard $cm^3$ $min^{-1}$.

The primary data in VENDAMS are the relative anion abundances ($Br^-$ from (5), $CF_3^-$ from (3), and $F^-$ from (4)) measured after a known reaction time (4.6 ms at 300 K, 1 Torr) as a function of the initial electron density at the neutral inlet ($[e^-]_0$). An example plot of data taken at 400 K and 1.33 Torr appears in Fig. 1; data at other temperatures and pressures are qualitatively similar. Rate constants are extracted from these data, from plots such as those shown in Fig. 2 produced using the Monte Carlo analysis procedure described below. At low $[e^-]_0$ ($[e^-]_0 < [CF_3Br]_0$), the primary electron attachment process (5) quickly depletes much of the electron density and secondary electron attachment (1)–(4) is not observable. As $[e^-]_0$ is increased, the concentrations of $F^-$ and $CF_3^-$ from secondary attachment increase relative to $Br^-$, reflecting both the rate and the product branching of electron attachment to $CF_3$. At very high $[e^-]_0$, above $10^{10}$ $cm^{-3}$, mutual neutralization of $CF_3^-$ with $Ar^+$ decreases the $CF_3^-$

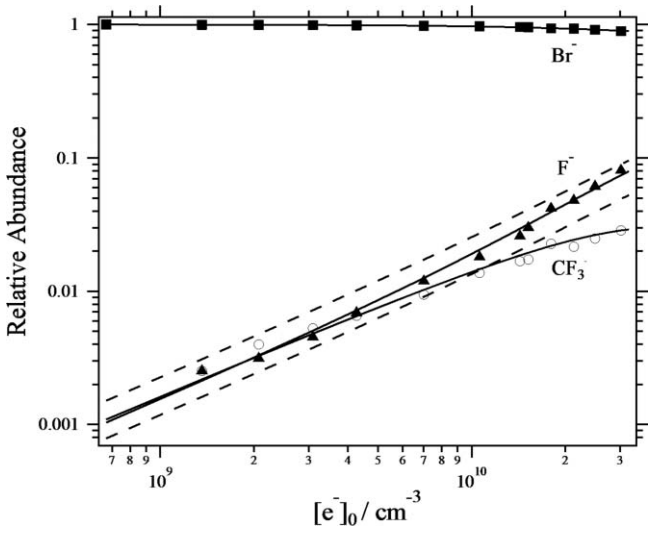


FIG. 1. Relative anion abundances 4.6 ms after the addition of $2.6 \times 10^{-9}$ cm$^{-3}$ $CF_3Br$ to the afterglow as a function of the initial electron density at 400 K and 1.33 Torr. Solid lines are best-fit calculated abundances (see text); dashed lines (shown only for $F^-$) are calculated abundances at the uncertainty limits of $k_{F^-}$.

abundance relative to the monatomic anions, which undergo neutralization with rate constants at least one order of magnitude smaller.[18]

The derivation of rate constants from the measured anion abundances has been described in detail in Ref. 6. The kinetics of the system is characterized by the known initial conditions throughout the known reaction time as described by the set of possible reactions between species known (observed ions) or inferred (corresponding neutrals) to be present in the flow tube. In addition to the electron attachment and mutual neutralization reactions described above, these include charge transfer from $Ar^+$ to neutral species including $H_2O$ and mutual neutralization of electrons and polyatomic cations. Although many reactions are included in the modeling, only the fastest reactions involving the most abundant species, namely, the electron attachment and mutual neutralization reactions described above have any measurable effect on the relative anion abundances. The rate constants of all reactions are varied using a Monte Carlo optimization procedure over ranges limited only by calculated collisional rate constants or, where possible, values from the literature. The procedure samples the full parameter space of the rate constants of all reactions. For each set of rate constants, the final anion abundances are calculated by iteratively solving the set of coupled differential equations describing the production and destruction of each species. The calculated abundances are compared to the experimental values via weighted least squares goodness-of-fit, with zero being a perfect fit. The best-fit value of each rate constant is determined by the minimum in a plot of the goodness-of-fit as a function of that particular rate constant, and uncertainty limits are determined by the extreme values of that rate constant yielding the worst goodness-of-fit that still provides a reasonable description of the data as judged by eye, see Fig. 2.

The current data determine the rate constants,

$$CF_3 + e^- \xrightarrow{k_{tot}} \text{products}, \tag{6}$$

$$CF_3 + e^- \xrightarrow{k_{CF_3^-}} CF_3^-, \tag{7}$$

$$CF_3 + e^- \xrightarrow{k_{F^-}} CF_2 + F^-. \tag{8}$$

It is important to note that the reported $k_{tot}$ are not determined simply by summing $k_{F^-}$ and $k_{CF_3^-}$ and convoluting the associated uncertainties, but rather more directly by the calculated goodness-of-fits as a function of $k_{tot}$. The distinction in results is subtle, but the uncertainties associated with the latter method are smaller. Additionally, it may be noted that the reported uncertainties in $k_{tot}$, $k_{F^-}$, and $k_{CF_3^-}$ are similar to, and in some cases smaller than the uncertainties in the literature value of the rate constant of electron attachment to $CF_3Br$ ($k_{CF_3Br}$). The uncertainty in the primary electron attachment rate constant is not fully propagated to the determined secondary rate constants because those determinations are much more sensitive to the relative concentrations of $Br^-$, $F^-$, and $CF_3^-$ than to their absolute concentrations. Regardless of the value of $k_{CF_3Br}$, the ratio of product $Br^-$ to product $CF_3$ is necessarily one. Our measured rate constants are summarized in Table I.

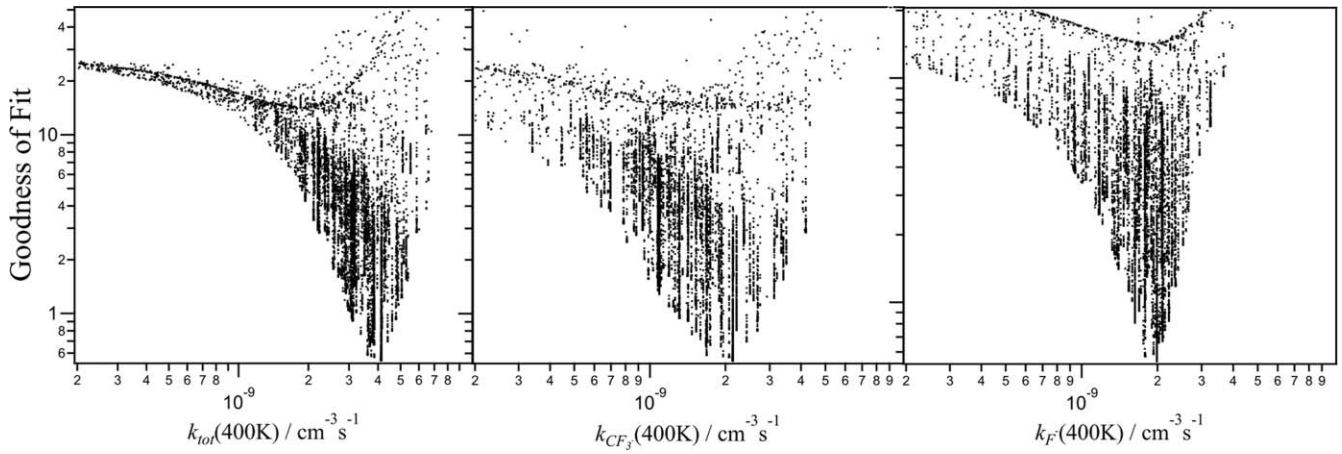


FIG. 2. Projections of the weighted least-squares goodness-of-fit of calculated to experimental anion abundances (see text), for the data shown in Fig. 1, on to three parameters ($k_{tot}$, $k_{CF_3^-}$, $k_{F^-}$) for which results are reported in this work.

TABLE I. Measured rate constants (with high and low uncertainty limits in parentheses) along with modeled rate constants (values behind the slash).

| | ($\times 10^{-9}$cm$^3$ s$^{-1}$) | | |
|---|---|---|---|
| 300 K Pressure (Torr) | $k_{tot}$ | $k_{CF_3^-}$ | $k_{F^-}$ |
| 0.75 | 2.8 (+1.7/−1.1)/2.9 | 1.9 (+1.5/−0.8)/2.3 | 0.8 (+0.3/−0.3)/0.6 |
| 1.0 | 3.4 (+2.1/−1.1)/3.5 | 2.7 (+2.2/−1.1)/3.0 | 0.6 (+0.3/−0.3)/0.6 |
| 1.8 | 7.2 (+5.5/−3.5)/5.2 | 6.1 (+5.5/−3.8)/4.7 | 1.0 (+0.4/−0.5)/0.6 |
| 2.0 | 6.5 (+2.7/−3.0)/5.7 | 5.8 (+2.6/−2.9)/5.2 | 0.7 (+0.3/−0.3)/0.7 |
| 400 K | | | |
| Pressure (Torr) | $k_{tot}$ | $k_{CF_3^-}$ | $k_{F^-}$ |
| 0.75 | 3.4 (+1.7/−1.7)/3.4 | 1.5 (+1.0/−0.9)/1.6 | 1.9 (+0.9/−1.0)/1.9 |
| 1.3 | 4.5 (+2.3/−2.0)/4.4 | 2.4 (+1.8/−1.3)/2.5 | 2.1 (+1.0/−1.0)/1.9 |
| 2.0 | 5.0 (+2.3/−2.3)/5.6 | 3.3 (+1.8/−1.8)/3.7 | 1.8 (+0.9/−0.8)/1.9 |
| 500 K | | | |
| Pressure (Torr) | $k_{tot}$ | $k_{CF_3^-}$ | $k_{F^-}$ |
| 0.8 | 4.3 (+1.3/−1.3)/4.5 | 1.4 (+0.8/−0.8)/1.0 | 2.8 (+1.4/−1.0)/3.5 |
| 1.0 | 5.0 (+2.0/−2.0)/4.8 | 1.7 (+0.9/−0.9)/1.3 | 3.0 (+1.1/−1.1)/3.5 |
| 1.67 | 5.1 (+1.4/−1.5)/5.7 | 1.4 (+1.1/−0.6)/2.2 | 3.6 (+1.1/−1.1)/3.5 |
| 2.0 | 6.9 (+3.5/−4.0)/5.9 | 3.0 (+2.0/−1.5)/2.4 | 3.9 (+1.8/−1.5)/3.5 |
| 600 K | | | |
| Pressure (Torr) | $k_{tot}$ | $k_{CF_3^-}$ | $k_{F^-}$ |
| 0.8 | 5.0 (+1.3/−1.6)/5.4 | 1.1 (+0.5/−0.5)/0.6 | 4.0 (+1.4/−1.6)/4.8 |
| 1.5 | 5.2 (+2.0/−2.0)/6.0 | 1.0 (+1.0/ −0.5)/1.2 | 4.2 (+1.7/ −2.0)/4.8 |
| 2.0 | 6.9 (+1.9/−2.1)/6.4 | 1.4 (+0.9/−0.8)/1.6 | 5.7 (+1.3/ −1.8)/4.8 |
| 2.5 | 6.9 (+2.0/−2.2)/6.7 | 2.0 (+1.2/−1.1)/1.9 | 4.0 (+1.7/−2.0)/4.8 |
| [He] = $3.2 \times 10^{16}$ cm$^{-3}$ | | | |
| $T$ (K) | $k_{tot}$ | $k_{CF_3^-}$ | $k_{F^-}$ |
| 300 | 3.4 (+2.1/−1.1)/3.5 | 2.7 (+2.2/−1.1)/3.0 | 0.6 (+0.3/−0.3)/0.6 |
| 400 | 4.5 (+2.3/−2.0)/4.4 | 2.4 (+1.8/−1.3)/2.5 | 2.1 (+1.0/−1.0)/1.9 |
| 500 | 5.1 (+1.4/−1.5)/5.7 | 1.4 (+1.1/−0.6)/2.2 | 3.6 (+1.1/ −1.1)/3.5 |
| 600 | 6.9 (+1.9/−2.1)/6.4 | 1.4 (+0.9/−0.8)/1.6 | 5.7 (+1.3/ −1.8)/4.8 |

Measurements were made from 300 to 600 K at pressures between 0.75 and 2.5 Torr. Figure 3 illustrates results as a function of temperature obtained at constant number density of [He] = $3.2 \times 10^{16}$ cm$^{-3}$. Measurements at various temperatures as a function of pressures between 0.70 and 2.0 Torr are shown in Figs. 4 and 5. The figures show the experimental points with their respective error bars together with modeled lines such as obtained by the kinetic modeling described in Secs. III and IV. One observes that the modeling well reproduces all details of the experimental results. The modeling serves two purposes. On one hand, it provides an understanding of the measured values of the rate constants $k_{tot}$, $k_{F^-}$, and $k_{CF_3^-}$ and their properties. On the other hand, it allows one to extend the present measurements far outside the applied conditions, which appear of interest for applications such as plasma etching.

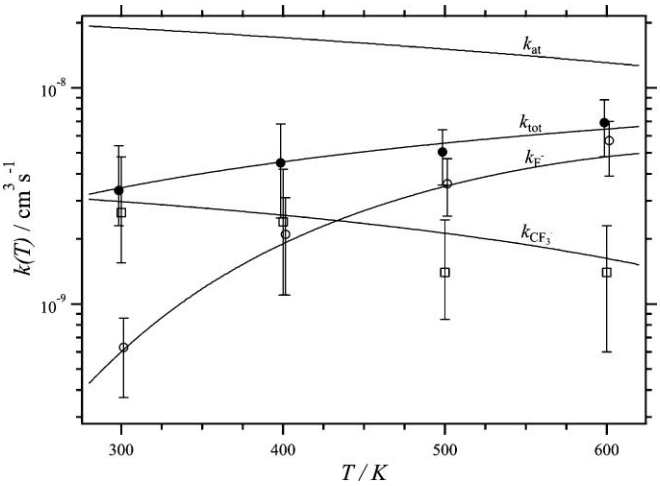


FIG. 3. Rate constants for total electron attachment to $CF_3$, $k_{tot}$, (full circles) and the competing dissociative, $k_{F^-}$, (open circles) and non-dissociative, $k_{CF_3^-}$, (open squares) product channels at $T = 300$ K. Some data points are slightly offset horizontally for clarity. Experimental data (symbols) and kinetic modeling (lines) are compared with modeled $k_{at}$, corresponding to primary attachment.

## III. KINETIC MODELING OF THE EXPERIMENTAL RESULTS

The observed temperature and pressure dependences of both the attachment rate coefficients and the $CF_3^-$ and $F^-$ branching fractions suggest that a quantitative analysis

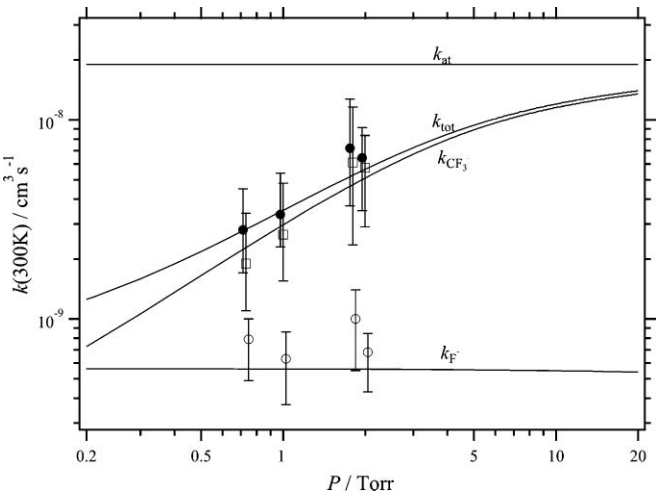


FIG. 4. Rate constants for total electron attachment to $CF_3$, $k_{tot} = k_{F^-} + k_{CF_3^-}$ (full circles), and the competing dissociative $k_{F^-}$ (open circles), and non-dissociative, $k_{CF_3^-}$ (open squares), product channels at $T = 300$ K. Some data points are slightly offset horizontally for clarity. Experimental data (symbols) and kinetic modeling (lines) are compared with modeled $k_{at}$, corresponding to primary attachment.

requires "kinetic modeling," such as we have employed earlier in our studies on the electron attachment to $SF_6$,[7–9] $SF_5Cl$,[19] $POCl_3$,[1–13] and $C_{60}$.[20] Each of these reactions had its specific features, and the present one adds another example to the combination of attachment and intrinsic reaction dynamics.

Our kinetic modeling is based on the mechanism of reactions (R1)–(R4) with their specific, energy dependent, rate constants symbolized as

$$CF_3 + e^- \xrightarrow{k_{at}} CF_3^{-*}, \tag{R1}$$

$$CF_3^{-*} \xrightarrow{k_{det}} CF_3 + e^-, \tag{R2}$$

$$CF_3^{-*} + M \xrightarrow{k_{stab}} CF_3^- + M, \tag{R3}$$

$$CF_3^{-*} \xrightarrow{k_{dis}} CF_2 + F^-. \tag{R4}$$

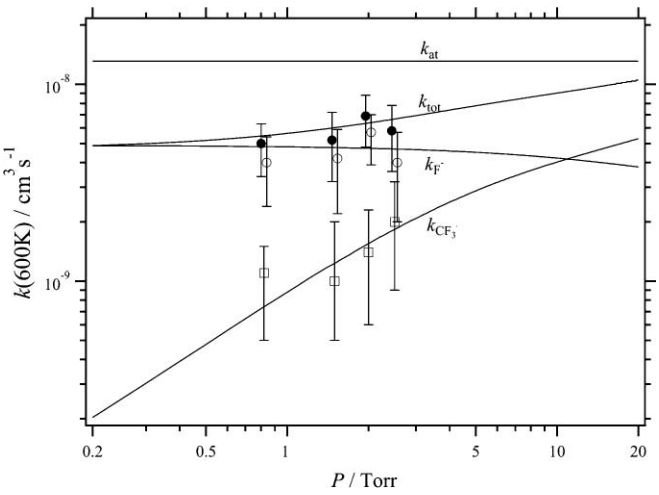


FIG. 5. As Fig. 4, but for $T = 600$ K.

Maximum $CF_3^-$ yields are obtained at pressures which are high enough that all excited $CF_3^{-*}$, formed by attachment (R1), is collisionally stabilized by step (R3). Complete collisional stabilization requires that the pseudo-first order rate constant $k_{stab}$ [M] of process (R3) is considerably larger than both the rate coefficients for electron detachment $k_{det}$ and for ion dissociation $k_{dis}$. The observation of a pressure dependence of the total rate coefficient $k_{tot}$ for electron attachment is an indication that this was not the case under the applied conditions. The kinetic modeling described in the following offers an opportunity to disentangle the mechanism and understand the observations in a quantitative way.

Under steady-state conditions for $CF_3^{-*}$, the mechanism of reactions (R1)–(R4) formally leads to the rate equations,

$$\begin{aligned} \frac{d[e^-]}{dt} &= \frac{d[CF_3]}{dt} = -k_{tot}[e^-][CF_3] \\ \frac{d[CF_3^-]}{dt} &= k_{CF_3^-}[e^-][CF_3] = Y_{CF_3^-}k_{at}[e^-][CF_3] \\ \frac{d[F^-]}{dt} &= k_{F^-}[e^-][CF_3] = Y_{F^-}k_{at}[e^-][CF_3] \end{aligned} \tag{9}$$

with the branching fractions

$$\begin{aligned} Y_{CF_3^-} &= \frac{k_{stab}\,[M]}{k_{det} + k_{dis} + k_{stab}\,[M]} \\ Y_{F^-} &= \frac{k_{dis}}{k_{det} + k_{dis} + k_{stab}\,[M]}. \end{aligned} \tag{10}$$

Since the sum of the $CF_3^-$ and $F^-$ branching fractions, $Y_{CF_3^-} + Y_{F^-}$, is smaller than unity when $k_{det}$ cannot be neglected, the total rate coefficient,

$$k_{tot} \approx k_{at}(Y_{CF_3^-} + Y_{F^-}) = \frac{k_{at}\,(k_{dis} + k_{stab}\,[M])}{k_{det} + k_{dis} + k_{stab}\,[M]} \tag{11}$$

is also smaller than $k_{at}$ and approaches the latter only at sufficiently large pressures, i.e., at sufficiently large buffer gas concentrations [M]. We, therefore, attribute the observed pressure dependence of $k_{tot}$ to the presence of the detachment step (R2).

The quantitative characterization of the overall rate coefficient $k_{tot}$ and the branching fractions $Y_{CF_3^-}$ and $Y_{F^-}$ requires information on the dependence of the primary attachment process on both the electron energy $E_{el}$ and the internal energy $E_{int}$ of the neutral target $CF_3$. We first assume that the two energy distributions are thermal and correspond to the same temperature $T_{el} = T_{gas} = T$. Neglecting rotational effects, we also identify the internal energy of $CF_3$ with its vibrational energy, $E_{int} = E_{vib}$. Furthermore, the specific rate constants $k_{det}(E)$, $k_{dis}(E)$, and $k_{stab}(E)$[M], with their dependences on the total internal energy $E = E_{el} + E_{vib}$ of the anion $CF_3^{-*}$ formed, need to be known. The chemical activation system of reactions (R1)–(R4) is treated by unimolecular rate theory combined with the specificities of the attachment step (R1). In particular, as we have emphasized before by demonstration for the $e^- + POCl_3$ system,[11] the intermediate $CF_3^{-*}$ in general does not have the same "internal temperature" as the electron and buffer gas temperatures $T_{el}$ and $T_{gas}$, respectively.

In the following, we briefly characterize the properties of the specific rate constants employed in our kinetic

modeling. The rate constants $k_{stab}(E)$ for collisional stabilization are represented by the Langevin rate constant $k_L = 2\pi e(\alpha/\mu)^{1/2}$ for collisions between $CF_3^{-*}$ and M = He (with the reduced mass $\mu$ and the polarizability $\alpha$ of M) multiplied by an effective collision efficiency $\gamma_c$. The latter depends[21] on the difference of the energy $E$ and the smaller of the threshold energies $E_{0,det}$ for electron detachment (R2) and $E_{0,dis}$ for fragmentation of $CF_3^{-*}$ (R4). In addition, it depends on the average energy $\langle\Delta E\rangle$ transferred per collision between $CF_3^{-*}$ and M = He (as well as on the energy dependences of $k_{det}(E)$ and $k_{dis}(E)$). As a result of solving the corresponding master equation, simplified expressions for the relation between $\gamma_c$ and $\min(E_{0,det},E_{0,dis})$, $\langle\Delta E\rangle$, $k_{det}(E)$, and $k_{dis}(E)$ were derived. Alternatively, one might also use a (down) step-ladder model for collisional deactivation such as we have done in our analysis of the electron attachment to $POCl_3$.[13] However, because up- and down-transitions turned out to be explicitly of importance, particularly for higher temperatures, the many-shot expansion technique from Ref. 22 appeared more appropriate for the present situation, see below.

The starting point for a quantitative representation of $k_{dis}(E)$ is phase space theory (PST) which provides an upper limit to $k_{dis}(E)$ and corresponds to free rotor transitional modes of the dissociating $CF_3^{-*}$. Expanding on this approach, we account for the partial rigidity of the transitional modes by a simplified statistical adiabatic channel model (SSACM) in the form derived in Refs. 23–25 and applied before[13] (for details, see Appendix). While $k_{stab}(E)$ contains $\langle\Delta E\rangle$ as a fit parameter, $k_{dis}(E)$ in the SSACM approach similarly contains one fit parameter, i.e., a "looseness parameter" $c_{loose}$, see, e.g., Refs. 13, 23, and 24. Unavoidably, one has to live at least with these two experimental fit parameters. However, they have to be within reasonable limits such as derived for other comparable systems.

The specific rate constants $k_{det}(E)$ for electron detachment from $CF_3^{-*}$, such as in our previous work,[5] are expressed by a combination of statistical unimolecular rate theory with state-specific transmission coefficients for the electron leaving the anion. The latter, through microscopic reversibility, are linked with the cross sections $\sigma_{at}$ for electron attachment.[5,8] The employed relationships are given in the Appendix.

The attachment rate constants $k_{at}$ follow from the product of the attachment cross section $\sigma_{at}$ and the electron velocity, averaged over a thermal electron velocity distribution. It may also depend on the vibrational states of $CF_3$ and be averaged over the thermal population of such states, such as this is the case for the present system, see below. In order to be able to perform the kinetic modeling, a suitable explicit expression for $\sigma_{at}$ needs to be formulated. We do this, first, by calculating $\sigma_{cap}$ for capture of electrons by polarizable dipolar neutral target molecules.[26] Recently, we have provided[27,28] approximate, analytical expressions for $\sigma_{cap}$ such as discussed in the Appendix. Using $\sigma_{cap}$ as a reference and upper limit for $\sigma_{at}$, we then express $\sigma_{at}$ in the form,[7]

$$\sigma_{at} = \sigma_{cap} P^{\mathrm{IVR}} \tag{12}$$

with an electron-phonon coupling (or intramolecular vibrational redistribution) factor $P^{\mathrm{IVR}}$. As the detailed calculation of $P^{\mathrm{IVR}}$ is cumbersome, we work with empirical and, therefore, still tentative expressions for $P^{\mathrm{IVR}}$. First, we factorize $P^{\mathrm{IVR}}$ into an electronic part $P^{\mathrm{IVR}}(E_{el})$ and into a nuclear part $P^{\mathrm{IVR}}(E_{n,p})$ the latter depending on the energy $E_{n,p}$ of the vibrational modes $p$ of the neutral target. In the simplest way, we employ an exponential trial function[7] for $P^{\mathrm{IVR}}(E_{el})$ and a nuclear factor $P^{\mathrm{IVR}}(E_{n,p})$ being unity at $E_{n,p}$ larger than a threshold energy $E_{n,0}$ and zero below, symbolically written as

$$P^{\mathrm{IVR}} \approx \exp(-E_{el}/E_{el}^*)[0,1], \tag{13}$$

$E_{n,0}$ is related to the crossing of ionic and neutral potential energy curves (see Ref. 26 and work cited therein) and the corresponding Franck-Condon factors, while $E_{el}^*$ is a constant fit parameter such as system-specifically determined before.[7,12] Underlying Eq. (13) is the simplifying assumption of Franck-Condon factors which are zero at $E_{n,p} < E_{n,0}$ and unity at $E_{n,p} \geq E_{n,0}$. As a consequence, the effective threshold energy for electron detachment in $k_{det}(E)$ is not the electron affinity EA of the neutral but the sum of EA and $E_{n,0}$, i.e.,

$$\mathrm{E}_{0,det} \approx \mathrm{EA} + \mathrm{E}_{n,0}. \tag{14}$$

Employing Eq. (13), in addition to the collisional energy transfer parameter $\langle\Delta E\rangle$ and dissociation looseness parameter $c_{loose}$, one has two more fit parameters, i.e., $E_{el}^*$ and $E_{n,0}$. Again, these parameters should be "reasonable" by being of similar magnitude as derived in kinetic modeling for other systems. It should be emphasized that Eq. (13) so far is a trial function only. In separate work, we tried to relate $P^{\mathrm{IVR}}$ to more detailed theories, such as R-matrix theory. From this work, we have evidence that the electronic factor $\exp(-E_{el}/E_{el}^*)$ might have to be replaced by an approximate factor $\exp[-(E_{el}/E_{el}^*)^{1/2}]$, i.e., instead of Eq. (13) $P^{\mathrm{IVR}}$ might have to be replaced by expressions such as

$$P^{\mathrm{IVR}} \approx \exp[-(E_{el}/E_{el}^*)^{1/2}][0,1]. \tag{15}$$

Therefore, we have done our kinetic modeling with either expressions for $P^{\mathrm{IVR}}$. It turned out that both approaches, with slightly modified parameters $E_{el}^*$, similarly well reproduce the experimental results.

Within the described simple model approach, the temperature dependence of $k_{at}$ stems from a combination of factors. There is first the contribution from the electron-dipole capture rate constant $k_{cap} = \langle\sigma_{cap}v_{el}\rangle$ ($\langle\ \rangle$ = thermal average, $v_{el}$ = electron velocity) which is known from Refs. 26–28. There is the additional dependence from the electronic part of $P^{\mathrm{IVR}}$ with the parameter $E_{el}^*$ and, finally, there is the nuclear factor related the parameter $E_{n,0}$. Experiments with independent variation of $T_{el}$ and $T_{gas}$ would provide a more direct access to these two fit parameters[12] than the present work with $T_{el} = T_{gas}$, in which $E_{el}^*$ and $E_{n,0}$ have to be fitted by the high-pressure extrapolated absolute value and temperature dependence of $k_{tot}$. As our database is limited, this fit is not unique and a variety of possibilities need to be explored, see below.

After having characterized the attachment rate constant $k_{at}$, one asks for its pressure and temperature dependent parts corresponding to redetachment of electrons, dissociation to $F^- + CF_2$, and collisional stabilization to $CF_3^-$. In order to obtain this information by kinetic modeling, one first needs

to know which fraction $g(E,T_{gas},T_{el})$ of $k_{at}$ initially leads to excited anions $CF_3^{-*}$ with a total internal energy $E = E_i + E_{el}$, where $E$ besides $E_{el}$ includes contributions from the thermal energy $E_i$ of $CF_3$. Following the corresponding treatment[13] in our work on electron attachment to $POCl_3$, we calculate

$$g\left(E, T_{gas}, T_{el}\right) \propto \sum_{E_i=0}^{E} P\left(E - E_i\right)\left(E - E_i\right)^{-1/2} \times \exp\left(-E_i / kT_{gas}\right) \exp\left[-\left(E - E_i\right) / kT_{el}\right], \tag{16}$$

where $g(E,T_{gas},T_{el})$ is a distribution per energy interval, and the summation goes over all vibrational levels $i$ of the vibrational mode $p$ of $CF_3$. $P(E - E_i)$ is given by the product of the transmission coefficient for the extended Vogt-Wannier electron-dipole capture model (see the Appendix), the electronic IVR factor $P^{\mathrm{IVR}}(E_{el} = E - E_i)$ and the nuclear IVR factor $P^{\mathrm{IVR}}(E_i)$ described above. If $E_{n,0}$ is related to one specific mode $p$, one also has to specify which of the vibrational modes of $CF_3$ is chosen as the "threshold-providing mode." While $E_{n,0} \approx 0$ was found empirically for $POCl_3$, the present system is different in having a threshold barrier for at least one of the modes. In agreement with $POCl_3^-$, the resulting energy distribution corresponds to a temperature $T_{eff}$, which differs from $T = T_{el} = T_{gas}$.

Once the initial distribution of vibrational energy $g(E,T_{gas},T_{el})$ of excited $CF_3^{-*}$ is known through Eq. (16), the time evolution of this distribution during the competing collisional energy transfer, electron detachment, and dissociation needs to be followed. Most generally, this requires the solution of the corresponding master equation, which leads to the energy-dependent branching fractions $Y_i$ for formation of $F^-$ and $CF_3^-$, respectively, as well as for detachment $Y_{det} = 1 - Y_{F^-} - Y_{CF_3^-}$. The $Y_i$ then are averaged over the distribution $g(E)$ through

$$\langle Y_i \rangle = \int_0^\infty g\left(E\right) Y_i\left(E\right) dE. \tag{17}$$

The $Y_i$ symbolically may be written as

$$Y_{F^-}\left(E\right) = \frac{k_{dis}(E)}{k_{dis}(E) + k_{det}(E) + \gamma_c(E) Z[\mathrm{M}]} \tag{18}$$

and the corresponding expressions for $Y_{CF_3^-}(E)$ and $Y_{det}(E)$. However, because of the highly structured character of $k_{dis}(E)$ and $k_{det}(E)$ illustrated below, the simplified expressions for the collision efficiencies $\gamma_c(E)$ from Ref. 21 cannot easily be used. One may also try to employ a step-ladder model with down steps, the latter given by the average total energy $\langle \Delta E \rangle$ transferred per collision. In this approach, one has

$$Y_{CF_3^-}\left(E\right) = \prod_{i=1}^{T(E)} \frac{Z\left[\mathrm{M}\right]}{Z\left[\mathrm{M}\right] + k_{dis}\left(E - (i-1)\left|\langle \Delta E \rangle\right|\right) + k_{det}\left(E - (i-1)\left|\langle \Delta E \rangle\right|\right)}, \tag{19}$$

where $T(E) = \mathrm{Integer}[(E - E_0)/|\langle \Delta E \rangle|] + 1$ denotes the number of steps needed for stabilization to energies below $E_0$, i.e., to the smaller of the threshold energies for dissociation and detachment. While this method works well for the lower temperatures of this work, it did not appear adequate for the higher temperatures, again because of the fine structures of $k_{dis}(E)$ and $k_{det}(E)$ combined with the importance of up transitions. On the other hand, again the fine structure made the full solution of the master equation unexpectedly cumbersome. For this reason, we returned to a method of intermediate complexity, the many-shot expansion technique[22] which was shown to converge to the solution of the master equation. In this case, the branching fractions are given by a series of nested summations. For example, for four shots one has

$$Y_{F^-}\left(E_i\right) = \left[\frac{k_{dis}\left(E_i\right)}{k_{dis}\left(E_i\right) + k_{det}\left(E_i\right)}\right]\left\{1 - \beta_i \sum_j P_{ji}\beta_j \times \left(\sum_l P_{lj}\beta_l \left(\sum_m P_{ml}\beta_m\right)\right)\right\} \tag{20}$$

with

$$\beta_i = \frac{Z[\mathrm{M}]}{Z[\mathrm{M}] + k_{dis}(E_i) + k_{det}(E_i)} \tag{21}$$

and with collisional transition probabilities $P_{ji}$ from energy $E_i$ to energy $E_j$ given by the exponential collision model of Ref. 32. Generally, 4–5 shots were sufficient to obtain converged results, see also the results of Ref. 22.

Total attachment rate constants and branching fractions were determined for the experimental temperatures and pressures in the described way for given sets of the parameters ($E_{el}^*$, $E_{n,0}$, $c_{loose}$, $\langle \Delta E \rangle$) together with a choice of the barrier-determining mode of $CF_3$. The results were found to depend on the individual parameters in various ways and with variable sensitivity. For instance, for the full set of observations, less good fits were obtained for strong collisions (i.e., $|\langle \Delta E \rangle| \gg kT_{gas}$) than for weak collisions. On the other hand, the looseness parameter $c_{loose}$ of the dissociation turned out to be relatively unimportant. The temperature dependence of the total, primary attachment rate constant $k_{at}$ was governed by the two counteracting effects of $E_{el}^*$ and $E_{n,0}$, larger $E_{n,0}$ lowering $k_{at}$ but leading to a positive temperature coefficient, larger $E_{el}^*$, on the other hand, lowering $k_{at}$ but leading to

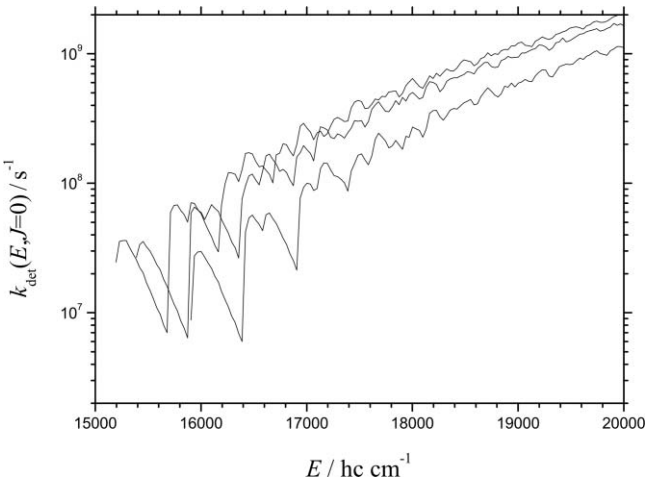


FIG. 6. Modeled specific rate constants $k_{det}(E)$ for electron detachment from $CF_3^{-*}$ (barrier-determining modes $\nu = 503$ cm$^{-1}$: left curve; 691 cm$^{-1}$: middle curve; 1224 cm$^{-1}$: right curve; see text).

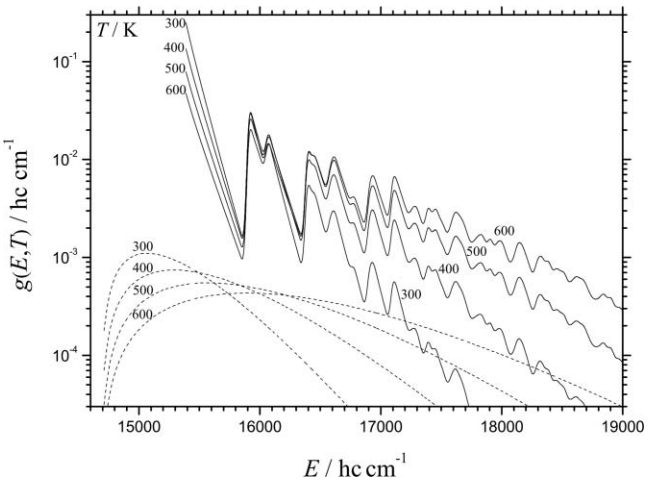


FIG. 8. Modeled distribution functions $g(E,T)$ of the internal energy $E$ of $CF_3^{-*}$ generated by thermal electron attachment to $CF_3$ (full lines) in comparison to thermal energy distributions of $CF_3$ (dashed lines) (with $P^{IVR}$ from Eq. (15) and the other parameters corresponding to the fit to the experiments shown in Figs. 3–5, see text, full lines shifted upward for clarity).

negative temperature coefficients. The influence of the two different expressions for the energy dependences of $P^{IVR}$ could easily be compensated by the choice of appropriate values of the parameters $E^*_{el}$ and $E_{n,0}$.

We do not document here the dependences of the modeling on the choice of the individual parameters but only present the final results, not without emphasizing that the fits are not completely unique. In Figs. 3–5, we have presented a comparison of the measured and modeled rate constant $k_{F^-}$, $k_{CF_3^-}$, and $k_{tot}$. The corresponding primary attachment rate constant $k_{at}$ is included. One realizes that $k_{tot} = k_{CF_3^-} + k_{F^-}$, because of the contribution of electron detachment, is markedly smaller than $k_{at} \cdot k_{tot}$ would approach $k_{at}$ only at pressures which are substantially larger than those applied in the present work. The resulting rate constants correspond to specific rate constants for dissociation $k_{det}(E)$ and for detachment $k_{dis}(E)$ such as illustrated in Figs. 6 and 7. In addition, Fig. 8 shows the populations $g(E,T)$ generated by the primary attachment process. Figures 3–8 correspond to the optimum parameter set, in cm$^{-1}$, of $(E^*_{el}, E_{n,0}, c_{loose}, -\langle\Delta E\rangle) = (67, 210, 100, 100)$ obtained by fitting the kinetic modeling to the experimental data (using IVR factors from Eq. (15) and employing the $CF_3$ oscillator with $\nu = 691$ cm$^{-1}$ as barrier-determining mode $p$, see above; the parameter $E^*_{el}$ corresponds to $P^{IVR}(E_{el}) = \exp(-c_1\kappa^2)$ with $c_1 \approx 24$ from Ref. 7). One notes the marked fine structure of $k_{dis}(E)$ and $k_{det}(E)$ reflecting the vibrational level structure of $CF_3$. It should be noted that Fig. 8, for illustration, shows $g(E,T)$ such as obtained with an integral over Whitten-Rabinovitch smoothed densities of states instead of the summation in Eq. (16). In the calculations, the true summation was used. In our work on electron attachment to $POCl_3$, we proceeded similarly.[13] In both cases, we observed that the effective temperature $T_{eff}$ of the anion generated by attachment was smaller than the gas temperature $T_{gas}$. In the present case, in addition, the threshold in the internal energy $E_{int} = E_{n,0}$ becomes apparent in Fig. 8.

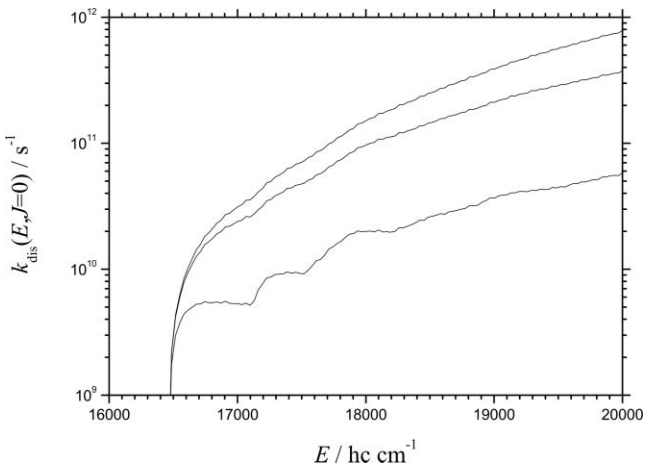


FIG. 7. Modeled specific rate constants $k_{dis}(E)$ for dissociation of $CF_3^{-*}$ to $F^- + CF_2$ (looseness parameter $c_{loose} = 100$ cm$^{-1}$: lower curve; $c_{loose} = 1000$ cm$^{-1}$: middle curve; $c_{loose} = \infty$(PST): upper curve; see text).

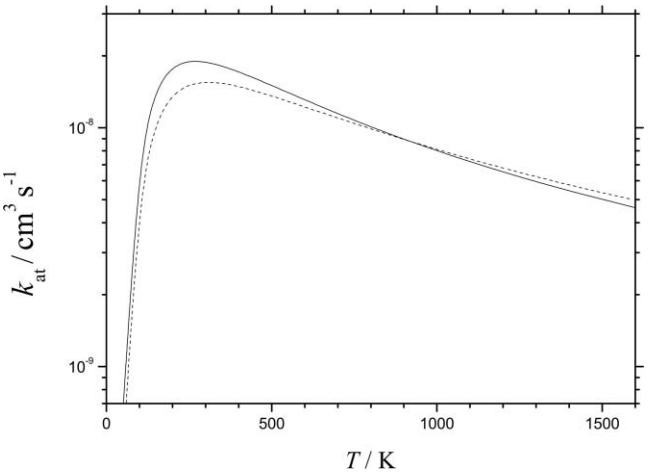


FIG. 9. Modeled primary attachment rate constants $k_{at}$ for $T_{gas} = T_{el}$ ($P^{IVR}$ from Eq. (13) with $E^*_{el} = 67$ cm$^{-1}$: full line; $P^{IVR}$ from Eq. (15) with $E^*_{el} = 33$ cm$^{-1}$; dashed line; the other parameters correspond to the fit to the experiments shown in Figs. 3–5).

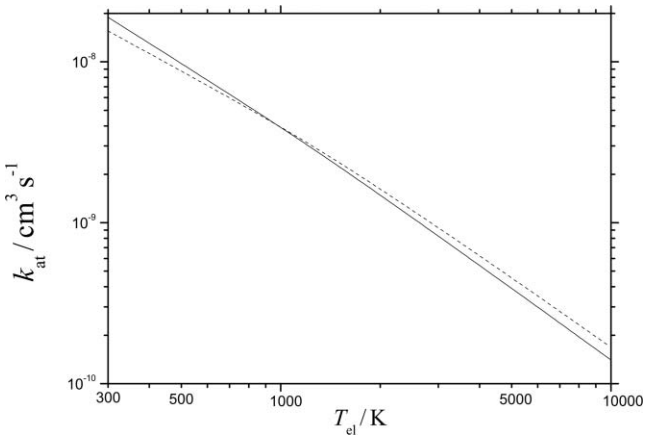


FIG. 10. As Fig. 9, but with fixed gas temperature $T_{gas} = 300$ K and variable electron temperature $T_{el}$.

It was emphasized above that the derived set of fit parameters is not completely unique and provides similarly good agreement with the experiments when varied within certain limits. Likewise, replacing Eq. (13) by Eq. (15) and using $E^*_{el} \approx 34$ cm$^{-1}$ instead of 67 cm$^{-1}$, similarly good agreement is obtained as with Eq. (13). In spite of the non-uniqueness of the fit, it can be used for predictions of $k_{CF_3^-}$ and $k_{F^-}$ outside the temperature and pressure ranges accessible in our experiments. It can also serve for modeling conditions when $T_{gas}$ and $T_{el}$ are not identical. These extensions of the kinetic modeling will be illustrated in Sec. IV.

## IV. PREDICTIONS FROM KINETIC MODELING

We have used the results of Sec. III in two ways to make predictions for conditions outside the accessible range. First, we extended the pressure and temperature ranges. Second, we also inspected the consequences of applying different gas and electron temperatures, $T_{gas}$ and $T_{el}$, respectively.

Figure 9 shows predicted primary attachment rate constants $k_{at}$ for $T_{gas} = T_{el}$ being varied over the range 300–2000 K. Results for the two different electronic IVR factors $P^{IVR}$ of Eqs. (13) and (15) are compared, leading to only minor differences. Figure 10 shows predictions of $k_{at}$ for $T_{gas} = 300$ K and $T_{el}$ varying independently over the range 300–10 000 K. The negative temperature coefficient of $k_{at}$ corresponds to that illustrated for electron attachment to $SF_6$ in Ref. 7. Over that large temperature range, differences for the two different expressions of $P^{IVR}$ naturally become apparent. Finally, Fig. 11 illustrates branching fractions $Y_{F^-}$ and $Y_{CF_3^-}$ as a function of pressure and temperature over wide ranges. The figure illustrates which pressures are needed to prevent detachment from reducing $k_{tot}$ below $k_{at}$; it also shows for which temperatures dissociation exceeds detachment. It was also found that, for fixed $T_{gas}$ and $T_{el}$ increasing up to 10 000 K, the branching fractions $Y_i$ in contrast to the values of $k_{at}$ varied only very slightly such that Fig. 11 can be used quite generally also for conditions with $T_{el} \neq T_{gas}$.

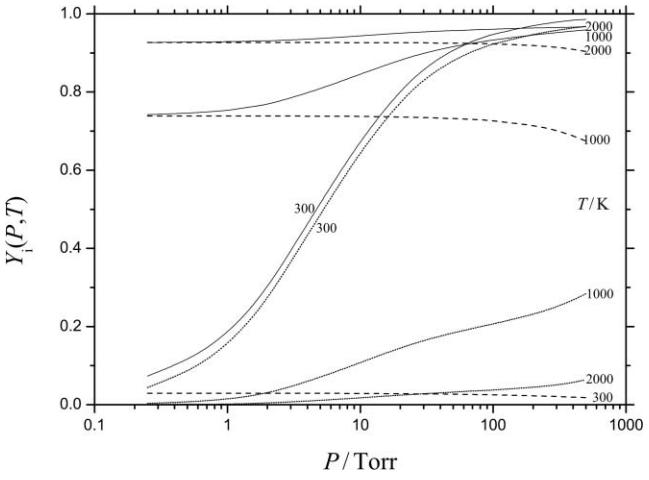


FIG. 11. Modeled branching fractions $Y_{F^-}$ (dashed lines), $Y_{CF_3^-}$ (dotted lines), and $Y_{tot} = Y_{F^-} + Y_{CF_3^-}$ (full lines) as a function of the bath gas (He) pressure and the temperature $T = T_{gas} = T_{el}$.

## V. CONCLUSIONS

Our experiments showed that $CF_3$ radicals in contrast to the predictions of Ref. 5 do undergo dissociative and non-dissociative electron attachment. The observed temperature and pressure dependences of the process indicate that dissociation, collisional stabilization, and electron detachment of the formed vibrationally excited $CF_3^{-*}$ anions are superimposed and all occur under the applied conditions. The results obtained offer the opportunity for a detailed analysis in terms of kinetic modeling on the basis of statistical unimolecular rate theory and statistical theory of electron attachment. With the smallest number of fit parameters possible, good agreement with the experimental data has been achieved. This allowed us to extrapolate the measurements far outside of the accessible experimental conditions, over wide temperature and pressure ranges as well as conditions with different electron and gas temperatures. The $CF_3$ system thus has become an example offering an unusual rich insight into the dynamics of dissociative electron attachment processes.

## ACKNOWLEDGMENTS

The project was funded by the United States Air Force of Scientific Research under Project No. 2303EP. Financial support by the European Office of Aerospace Research and Development (Grant No. FA8655-10-1-3057) is also acknowledged. T.M.M. is under contract (No. FA8718-10-C-0002) from the Institute for Scientific Research of Boston Colleagues. A.I.M. gratefully acknowledges support by the Deutsche Forschungsgemeinschaft (TR 69/17-2).

## APPENDIX: MODELING DETAILS OF RATE CONSTANTS

1. *Capture cross sections:* Following Ref. 28, capture cross sections are calculated taking into account a dipole moment of $CF_3$ of $\mu_D = 0.43$ ($\pm 0.07$) D from Refs. 5 and 33 and a polarizability of $CF_3$ of $\alpha = 3.4 \times 10^{-24}$ cm$^3$ (estimated as one half of the value[34] of $C_2F_6$). The reduced dipole parameter is $d = q\mu\mu_D/\hbar^2 = 0.169$; the reduced wave vector is $\kappa = \mu q(2\alpha E_{el})^{1/2}/\hbar^2 = 1.3(E_{el}/\text{eV})^{1/2}$; according to Fig. 2 of Ref. 28, the

capture probability $P_{0,0}(\kappa,d)$ within accuracy agrees with $P_0(\kappa)$ for s waves and nonpolar targets such as given by $P_0(\kappa) \approx 1 - 0.25\ \exp(-1.41\ \kappa) - 0.75\ \exp(-4.86\ \kappa)$. The capture cross section then is given by $\sigma_{cap}(E_{el}) \approx P_0(E_{el})\pi\hbar^2/(2\mu E_{el}) = 1.197 \times 10^{-15}\ \mathrm{cm}^2\ P_0(E_{el})\ (E_{el}/\mathrm{eV})^{-1}$.

2. *Specific rate constants for detachment and dissociation:* Vibrational frequencies (in $\mathrm{cm}^{-1}$): $CF_3$: 503, 503, 691, 1063, 1222, 1224; $CF_3^-$: 435, 435, 594, 731, 736, 948; $CF_2$: 667, 1085, 1209. Rotational constants (in $\mathrm{cm}^{-1}$): $CF_3$: 0.360, 0.360, 0.186; $CF_3^-$: 0.333, 0.332, 0.183; $CF_2$: 2.889, 0.414, 0.364. Vibrational frequencies and rotational constants are from density functional theory (DFT) calculations (B3LYP/6–311+G(d), GAUSSIAN 03).

   Energies (at 0 K, in eV): $CF_3^- \rightarrow CF_3 + e^-$: EA $= +1.820\ (\pm 0.05)$ from Ref. 14; $CF_3 + e^- \rightarrow CF_2 + F^-$: $+0.22\ (\pm 0.02)$, from Ref. 15.

   Specific rate constants $k(E)$ for detachment and dissociation through statistical theory are given by $k(E) = W(E)/\mathrm{h}\rho(E)$ ($J$ dependences are neglected). Vibrational densities of states $\rho(E)$ are determined by state counting. For detachment, $W(E)$ is given by $W_{det}(E) = \sum_i P(E - E_{0i})$ where $E - E_{0i} = E_{el,i}$, the summation extends over all vibrational energy levels $E_{0i}$ of $CF_3$ and the $P(E - E_{0i})$ are related to attachment cross sections $\sigma_{at}(E_{el,i})$ through $P(E_{el,i}) = \sigma_{at}(E_{el,i}){k_{p,i}}^2/\pi$ with $k_{p,i} = [2\mu(E - E_{0,i})]^{1/2}/\hbar$, see Ref. 7. For dissociation, $W(E)$ is approximated by the SSACM in which $W(E)$ denotes the number of open channels; the threshold energies for conserved modes are given by the vibrational modes of $CF_2$; the numbers of open channels for transitional modes are given by $W^{trans}(E) = f_{rigid}^{trans}(E)W^{trans,\mathrm{PST}}(E)$ with rigidity factors of the simplified form $f_{rigid}^{trans} \approx (1 - f_\infty)\ \exp[-(E - E_{0,dis})/c_{loose}] + f_\infty$, see Refs. 13, 23–25; $W^{trans,\mathrm{PST}}(E)$ is from Ref. 33 for spherical top + atom dissociation products.

3. The total rate constant for collisional energy transfer, i.e., the Langevin rate constant $k_L = 2\pi e(\alpha/\mu)^{1/2}$, for $CF_3$ + He collisions is estimated as $5.45 \times 10^{-10}\ \mathrm{cm}^3\ \mathrm{molecule}^{-1}\ \mathrm{s}^{-1}$.


[1] L. G. Christophorou and J. K. Olthoff, *Fundamental Electron Interactions with Plasma Processing Gases* (Kluwer Academic/Plenum, New York, 2004).
[2] P. Chabert, H. Abada, J.-P. Booth, and M. Lieberman, J. Appl. Phys. **94**, 76 (2003).
[3] K. Graupner, T. A. Field, and C. A. Mayhew, New J. Phys. **12**, 083035 (2010).
[4] D. Hayashi, Jpn. J. Appl. Phys. **43**, 2711 (2004).
[5] I. Rozum, N. J. Mason, and J. Tennyson, New J. Phys. **5**, 155 (2003).
[6] N. S. Shuman, T. M. Miller, C. M. Caples, and A. A. Viggiano, J. Phys. Chem. A **114**, 11100 (2010).
[7] J. Troe, T. M. Miller, and A. A. Viggiano, J. Chem. Phys. **127**, 244303 (2007).
[8] J. Troe, T. M. Miller, and A. A. Viggiano, J. Chem. Phys. **127**, 244304 (2007).
[9] A. A. Viggiano, T. M. Miller, J. F. Friedman, and J. Troe, J. Chem. Phys. **127**, 244305 (2007).
[10] J. Troe, T. M. Miller, and A. A. Viggiano, J. Chem. Phys. **130**, 244303 (2009).
[11] J. M. van Doren, J. F. Friedman, T. M. Miller, A. A. Viggiano, S. Denifl, P. Scheier, T. D. Märk, and J. Troe, J. Chem. Phys. **124**, 124322 (2006).
[12] N. S. Shuman, T. M. Miller, A. A. Viggiano, and J. Troe, "Electron attachment to $POCl_3$. II. Dependence of the attachment rate coefficients on gas and electron temperature," Int. J. Mass Spectrom. (in press).
[13] N. S. Shuman, T. M. Miller, A. A. Viggiano, and J. Troe, J. Chem. Phys. **134**, 094310 (2011).
[14] H.-J. Deyerl, L. S. Alconel, and R. E. Continetti, J. Phys. Chem. A **105**, 552 (2001).
[15] J. Csontos, Z. Rolik, S. Das, and M. Kállay, J. Phys. Chem. A **114**, 13093 (2010).
[16] W. C. Lineberger and L. J. Puckett, Phys. Rev. **186**, 116 (1969).
[17] S. Marienfeld, T. Sunagawa, I. I. Fabrikant, M. Braun, M.-W. Ruf, and H. Hotop, J. Chem. Phys. **124**, 154316 (2006).
[18] J. J. Church and D. Smith, J. Phys. D **11**, 2199 (1978).
[19] J. M. van Doren, T. M. Miller, A. A. Viggiano, P. Španěl, D. Smith, J. C. Bopp, and J. Troe, J. Chem. Phys. **128**, 094309 (2008).
[20] A. A. Viggiano, J. F. Friedman, N. S. Shuman, T. M. Miller, L. C. Schaffer, and J. Troe, J. Chem. Phys. **132**, 194307 (2010).
[21] J. Troe, J. Phys. Chem. **87**, 1800 (1983).
[22] R. V. Serauskas and E. W. Schlag, J. Chem. Phys. **42**, 3009 (1965).
[23] J. Troe and V. G. Ushakov, J. Phys. Chem. A **110**, 6732 (2006).
[24] W. Stevens, B. Sztaray, N. S. Shuman, T. Baer, and J. Troe, J. Phys. Chem. A **113**, 573 (2009).
[25] J. Troe, Z. Phys. Chem. **223**, 347 (2009).
[26] I. I. Fabrikant and H. Hotop, Phys. Rev. A **63**, 022706 (2001).
[27] E. I. Dashevskaya, I. Litvin, E. E. Nikitin, and J. Troe, Phys. Chem. Chem. Phys. **10**, 1270 (2008).
[28] E. I. Dashevskaya, I. Litvin, E. E. Nikitin, and J. Troe, J. Phys. Chem. A **115**, 6825 (2011).
[29] I. I. Fabrikant and H. Hotop, J. Chem. Phys. **128**, 124308 (2008).
[30] K. Aflatooni and P. D. Burrow, J. Chem. Phys. **113**, 1455 (2000).
[31] H. Hotop, M.-W. Ruf, J. Kopyra, T. M. Miller, and I. I. Fabrikant, J. Chem. Phys. **134**, 064303 (2011).
[32] J. Troe, J. Chem. Phys. **66**, 4745 (1977).
[33] N. I. Butkovskaya, M. N. Larichev, I. O. Leipunski, I. I. Morozov, and V. L. Talrose, Chem. Phys. Lett. **63**, 375 (1979).
[34] T. M. Miller, in *Handbook of Chemistry and Physics*, 85th ed., edited by D. R. Lide (CRC, Boca Raton, FL, 2004).
[35] J. Troe, J. Chem. Phys. **79**, 6017 (1983).